JOURNAL OF COMPUTATIONAL PHYSICS 64, 443–458 (1986)

Collocation for an Integral Equation Arising in Duct Acoustics*

WILLIAM F. MOSS

Department of Mathematical Sciences, Clemson University, Clemson, South Carolina 29631

Received February 28, 1984; revised May 13, 1985

A model has been developed for spinning mode acoustic radiation from the inlet of an aircraft engine. Consider the region bounded by the z-axis and the curve $PABCDEF$ in Fig. 2. The model inlet is the solid of revolution obtained by rotating this region about the z-axis. The circular disk $S1$ generated by rotating the line segment $C1 = 0B$ separates the interior of the inlet from its exterior. The interior acoustic pressure consists of a pure azimuthal mode for a hardwall boundary condition. The interior and exterior acoustic pressures and their normal derivatives are matched on $S1$. A hardwall boundary condition is applied on the surface $S2$ generated by rotating the curve $C2 = BCDEF$. The governing boundary value problem for the Helmholtz equation is first converted into an integral equation for the unknown acoustic pressure on $S1 + S2$, and then the azimuthal dependence is integrated out yielding a one-dimensional integral equation over $C1 + C2$. We approximate the pressure on $C1$ by a truncated interior modal expansion and on $C2$ by a linear spline.

1. INTRODUCTION

Methods to suppress aircraft engine noise have included the development of acoustics linears, high Mach number inlets, and the use of inlet geometry to redirect the sound. Experiments with and without flow have been conducted at Langley Research Center [1, 2] to study these methods. In particular, in July of 1982 Richard Silcox [2] examined the effect of inlet geometry on the reflected and radiated acoustic fields; this paper describes a mathematical model for the no-flow experiments.

The experiments of Silcox were designed around the spinning mode synthesizer (SMS). Figure 1 shows a plan view of this facility in the Langley Research Center Aircraft Noise Reduction Laboratory. The SMS can excite a nearly pure (20–30 dB isolation) azimuthal mode inside the hard cylindrical duct which pierces the wall of the anechoic room. By attaching various test inlets to the end of this duct, inlet geometry can be varied.

* Research was supported by the National Aeronautics and Space Administration under NASA Contracts NAS1-17130 and NAS1-16394 while the author was in residence at the Institute for Computer Applications in Science and Engineering, NASA Langley Research Center, Hampton, Va. 23665.

0021-9991/86 $3.00

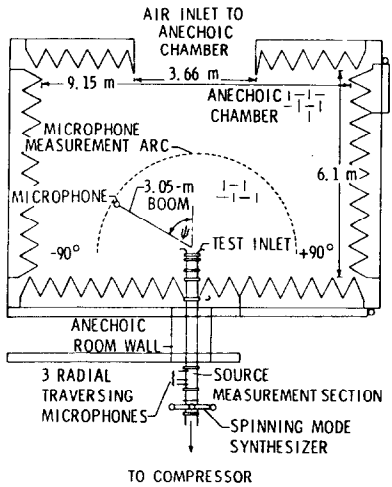

FIG. 1. Plan view of SMS/flow duct facility in Aircraft Noise Reduction Laboratory.

We attempt to retain the essential features of this experiental setup in our model inlet. Consider the region bounded by the z-axis and the curve $PABCDEF$ in Fig. 2. The model inlet is the solid of revolution obtained by rotating this region about the z-axis. The circular disk $S1$ generated by rotating the line segment $C1 = 0B$ separates the interior of the inlet from its exterior. The experimental test inlet is modeled by the surface produced by rotating the curve BCD. The revolution of DEF generates a termination for the model inlet. We denote by $S2$ the surface obtained by rotating $C2 = BCDEF$.

To model the SMS the acoustic pressure in the interior of the inlet consists of a pure, cylindrical azimuthal mode for the Helmholtz equation with hardwall boundary condition. In the exterior region the pressure is required to satisfy the Helmholtz equation and the radiation condition at infinity. The interior and exterior pressures and their normal derivatives are matched on $S1$. A hardwall boundary condition is applied on $S2$. This boundary value problem is converted

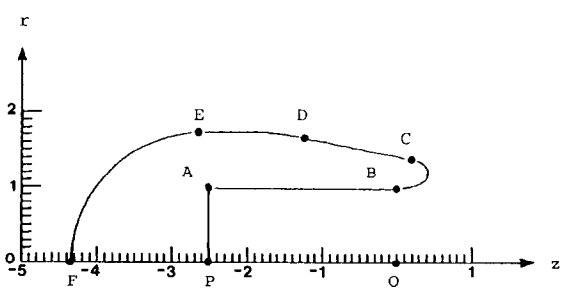

FIGURE 2

into an integral equation over $S1 + S2$ using Helmholtz' formula. The unknowns in the equation are the complex pressure on $S2$ and the reflection coefficients in the interior modal expansion. By assuming a pure azimuthal mode excitation, it is possible to integrate out the azimuthal dependence which yields a one-dimensional integral equation at the expense of a somewhat more complicated kernel. This model was suggested by the aproach of Kagawa *et. al.* [5] to loudspeaker design.

We note that uniqueness holds for the boundary value problem if the surface generated by *ABCDEF* is smooth (see Section 6); however, uniqueness does not hold for the integral equation if the wave number of the excitation is an eigenvalue for the Helmholtz equation in the interior of $S1 + S2$ with Dirichlet boundary condition. Numerically, we observe that, when discretized, the resulting linear system becomes increasingly ill-conditioned as an interior eigenvalue is approached. One effective method of removing this difficulty is to replace the free space Green's function in Helmholtz' formula by a modified Green's function (see [16–19], see also [14, 15]). Since the wave numbers of interest did not yield ill-conditioned linear system in our work, we did not use the modified Green's function approach.

The numerical method used is collocation. The unknown pressure on $C1$ (and its normal derivative) is approximated by a finite Bessel series which is a truncation of the interior modal expansion. The unknown pressure on $C2$ is approximated by a linear spline. The absolute error in the solution is estimated at the knots of the spline and this information is used to recommend the number of knots required for a given error tolerance on $C2$. This information can also be used to distribute the recommended number of knots to achieve an equal distribution of the absolute error. This is useful if it should be necessary to run the code a second time in order to achieve a better error performance. The code also provides (optionally) for one step of Neumann iteration. This yields a natural interpolation formula for the pressure and gives an approximation with the same smoothness as the exact solution. Finally, Helmholtz' formula is used to compute the pressure on a semicircle in front of the inlet for comparison with experimental results.

This paper explores numerically the nonstandard boundary value problem generated by our model, the knot redistribution scheme suggested by a theorem of de Boor, and the use of a two-dimensional adaptive integrator to estimate the oscillatory and sometimes singular integrals that arise. We point out that duct acoustics has been studied extensively in recent years. The reader is referred to [3] for a bibliography and a discussion of the various numerical methods which have been used.

2. The Model

Let a denote the interior radius ($a = 0.15$ m) of the test inlet in Fig. 1 and introduce a cylindrical coordinate system $(\bar{z}, \bar{r}, \theta)$ with origin 0 and positive $\bar{z}$-axis pointing out of the model inlet. Let ω denote the angular frequency of the

excitation, c the speed of sound, and $\bar{k} = \omega/c$ the reduced wave number. We will use the dimensionless coordinates $z = \bar{z}/a$ and $r = \bar{r}/a$ and the parameter $k = \bar{k}a$. The model inlet in the (z, r, θ) coordinate system is indicated in Fig. 2. As explained in Section 1, the circular disk $S1$ is obtained by rotating the line segment $C1 = 0B$ about the z-axis, while surface $S2$ is obtained by rotating $C2 = BCDEF$ about the z-axis. In this section we will assume that the surface generated by rotating $ABCDEF$ about the z-axis is C^1.

Let Ω denote the exterior of $S1 + S2$ and let D denote the interior of $S1 + S2$. We denote complex pressure by $\Phi(z, r, \theta)\, e^{-i\omega t}$ where

$$\begin{aligned} \Phi &= \phi, \qquad z(A) \leqslant z \leqslant 0,\ r \leqslant 1 \\ &= \psi, \qquad \text{in } \Omega, \end{aligned}$$

where $z(A) < 0$ denotes the z-coordinate of point A in Fig. 2. We note that the acoustic pressure obtained by this model is independent of $z(A)$. For a fixed positive integer m, we model the SMS by using the modal expansion $\phi = \bar{\phi} e^{im\theta}$ with

$$\bar{\phi} = \sum_{n=0}^{\infty} (A(n)\, e^{iL(n)z} + R(n)\, e^{-iL(n)z})\, J_m(\lambda(n)\, r). \tag{2.1}$$

This expansion comes from separation of variables in the reduced wave equation plus application of the hardwall boundary condition. In practice other "m" or azimuthal modes are present inside the duct but are at least 20 dB below the desired mode. In (2.1) J_m denotes the ordinary Bessel function of the first kind and order m. The increasing sequence $\lambda(n)$ is defined by $J'_m(\lambda(n)) = 0$, $n \geqslant 0$. We assume that $k \neq \lambda(n)$ for all n and define NCT to be the integer satisfying $\lambda(\text{NCT} - 1) < k < \lambda(\text{NCT})$. Then

$$\begin{aligned} L(n) &= (k^2 - (\lambda(n))^2)^{1/2}, \qquad 0 \leqslant n \leqslant \text{NCT} - 1 \\ -iL(n) &= ((\lambda(n))^2 - k^2)^{1/2}, \qquad n \geqslant \text{NCT}. \end{aligned} \tag{2.2}$$

The radial modes corresponding to $n = 0, \ldots, \text{NCT} - 1$ are called cuton, the other cutoff, and NCT is the number of cuton radial modes. Complex $R(n)$ is called the reflection coefficient of the nth radial mode, while complex $A(n)$ is the amplitude of the forward propagating modes, since we assume that $A(n) = 0$ for $n \geqslant \text{NCT}$. This is a reasonable assumption since the plane of the 24 acoustic drivers of the SMS is about 13 duct interior diameters from the mouth of the experimental duct. We assume that the amplitudes $A(n)$ are known for $0 \leqslant n \leqslant \text{NCT} - 1$; i.e., in a given experiment this data is available from the SMS. The reflection coefficients $R(n)$, $n \geqslant 0$, are unknowns. We note that the dependence on m in the above notation has been suppressed.

The appropriate boundary value problem for the Helmholtz equation (the wave equation with the harmonic time dependence separated out) can be stated as follows:

Find ψ in class $C^2(\Omega) \cap C^1(\bar{\Omega})$ such that $\Delta\psi + k^2\psi = 0$ in Ω,

$$\frac{\partial \psi}{\partial \eta} = 0 \qquad \text{on } S2, \tag{2.3}$$

ψ satisfies the radiation condition at infinity, $\psi = \phi$, and $\partial\psi/\partial z = \partial\phi/\partial z$ on $S1$.

We use Helmholtz' formula (an application of Green's third identity) to convert (2.3) into an integral equation (see [6]). Let $\mathbf{x}$ denote the observation point and $\mathbf{x}'$ the integration point. Then

$$\begin{aligned}
&\psi(\mathbf{x}) \cdot 4\pi, && \mathbf{x} \in \Omega \\
&\quad \cdot 2\pi, && \mathbf{x} \in S1 + S2 - (S1 \cap S2) \\
&\quad \cdot \pi, && \mathbf{x} \in S1 + S2 \\
&\quad \cdot 0, && \mathbf{x} \in D \\
&= \int_{S1+S2} \left(\frac{\partial \psi}{\partial \eta'}(\mathbf{x}') \frac{e^{ik\bar{R}}}{\bar{R}} - \psi(\mathbf{x}') \frac{\partial}{\partial \eta'} \left(\frac{e^{ik\bar{R}}}{\bar{R}} \right) \right) dS',
\end{aligned} \tag{2.4}$$

where $\bar{R} = |\mathbf{x} - \mathbf{x}'|$. Here η' denotes the normal to $S1 + S2$ pointing into D. Now uniqueness for (2.3) implies that $\psi = \bar{\psi}(z, r)\, e^{im\theta}$. If we change to cylindrical coordinates in (2.4), multiply by $e^{-im\theta}$, and integrate from $\theta = -\pi$ to $\theta = \pi$, we obtain the one-dimensional integral equation

$$\left.\begin{aligned}
&\bar{\psi}(z, r), && (z, r) \in C2 - (C1 \cap C2) \\
&\bar{\psi}(z, r)/2, && (z, r) = C1 \cap C2 \\
&\bar{\phi}(z, r), && (z, r) \in C1
\end{aligned}\right\} = -\int_0^1 r'\, dr' \frac{\partial}{\partial z'} \bar{\phi}(0, r')\, K(z, r; 0, r')$$

$$+ \int_0^1 r'\, dr'\, \bar{\phi}(0, r') \frac{\partial K}{\partial z'}(z, r; 0, r')$$

$$- \int_{C2} r'\, ds'\, \bar{\psi}(z', r') \frac{\partial K}{\partial \eta'}(z, r; z', r'), \tag{2.5}$$

where

$$K(z, r; z', r') = \pi^{-1} \int_0^{\pi} \cos(mY) \frac{e^{ikR}}{R}\, dY, \tag{2.6}$$

$$R = ((z - z')^2 + (r - r')^2 + 4rr' \sin^2(Y/2))^{1/2}, \tag{2.7}$$

s' denotes arc length on $C2$, and η' denotes the normal to $C2$ pointing toward the inlet interior. We note that (2.5) appears to be homogeneous; however, $\bar{\phi}$ in (2.1) is the sum of two terms, one of which is assumed known. This is the excitation term

$$\sum_{n=0}^{\infty} A(n)\, e^{iL(n)z}\, J_m(\lambda(n)\, r)$$

controlled by the SMS.

3. The Numerical Method

Our numerical method is collocation. We require (2.5) to hold at specified (collocation) points on $C1 + C2$. We obtain a full, square complex linear system whose solution provides an approximate solution to (2.5).

For the approximation of $\bar{\phi}$ we truncate (2.1) at $n = N1 > \mathrm{NCT} - 1$,

$$\bar{\phi} \simeq \sum_{n=0}^{N1} (A(n)\, e^{iL(n)z} + R(n)\, e^{-iL(n)z})\, J_m(\lambda(n)\, r). \tag{3.1}$$

To approximate $\bar{\psi}$ on $C2$, we first parameterize this contour. We will refer to certain values of this parameter t as knots. We require points B, C, D, E, and F to be knots. Additionally, knots are added so that BC is divided into $K2$ subintervals of equal length with respect to this parameter, CD into $K3$ subintervals, DE into $K4$ subintervals, and EF into $K5$ subintervals. This yields $N2 + 1 = K2 + K3 + K4 + K5 + 1$ knots.

We use $N2$ Chapeau functions, $\bar{\psi}_n(s)$ depending on arc length s, to approximate $\bar{\psi}$. These basis functions are centered at the values of s corresponding to the knots, except for the knot corresponding to the endpoint F of $C2$. This is because the solution at F must be zero for azimuthal mode index $m \geqslant 1$. Hence, we write

$$\bar{\psi} \simeq \sum_{n=N1+1}^{N1+N2} C(n)\, \bar{\psi}_n(s) \qquad \text{on } C2. \tag{3.2}$$

We have experimented with two numerical procedures.

I. (i) Collocate at $(0, r_0),\ldots, (0, r_{N1})$ where $0 < r_0 < \cdots < r_{N1} < 1$ satisfy $J_m(\lambda(N1 + 1)\, r_i) = 0$; i.e., choose the r coordinates to be positive zeros of the first term left out in the truncation (3.1) with $z = 0$.

(ii) Collocate at the points $(z_{N1+1}, r_{N1+1}),\ldots, (z_{N1+N2}, r_{N1+N2})$ corresponding to the centers of the Chapeau functions.

II. (i) As in I.

(ii) As in I but replace the equation generated by the collocation point at B by the continuity equation

$$-\sum_{n=0}^{N1} R(n)\, J_m(\lambda(n)) + C(N1 + 1) = \sum_{n=0}^{N1} A(n)\, J_m(\lambda(n)). \tag{3.3}$$

Now let $\mathbf{R} = [R(0),\ldots, R(N1)]^{\mathrm{T}}$, $\mathbf{C} = [(N1 + 1),\ldots, C(N1 + N2)]^{\mathrm{T}}$, and $\mathbf{A} = [A(0),\ldots, A(N1)]^{\mathrm{T}}$. We write the linear system resulting from I or II by

$$\mathrm{CKTOT}^*[\mathbf{R}, \mathbf{C}]^{\mathrm{T}} = \mathrm{CRITE}^*\mathbf{A}, \tag{3.4}$$

where CKTOT is a full, complex square matrix of order $N1 + N2 + 1$ and CRITE is

an $(N1+1)\times(N1+N2+1)$ complex matrix. Writing (3.4) in block form for procedure I we have

$$\left[\begin{array}{c|c} \mathscr{A}+\mathscr{B} & \mathscr{C} \\ \hline \mathscr{E}+\mathscr{F} & \mathscr{D}+\mathscr{G} \end{array}\right]\left[\begin{array}{c} \mathbf{R} \\ \hline \mathbf{C} \end{array}\right]=\left[\begin{array}{c} \mathscr{B}-\mathscr{A} \\ \hline \mathscr{E}-\mathscr{F} \end{array}\right]\mathbf{A}, \tag{3.5}$$

where

$$\mathscr{A}(l,n)=J_m(\lambda(n)\,r_l), \qquad 0\leqslant l,n\leqslant N1, \tag{3.6}$$

$$\mathscr{B}(l,n), \qquad 0\leqslant l,n\leqslant N1$$

$$\mathscr{E}(l,n), \qquad N1+1\leqslant l\leqslant N1+N2,\ 0\leqslant n\leqslant N1$$

$$=-iL(n)\int_0^1 r'\,dr'\,J_m(\lambda(n)\,r')\,K(z_l,r_l;0,r'), \tag{3.7}$$

$$\mathscr{F}(l,n)=-\int_0^1 r'\,dr'\,J_m(\lambda(n)\,r')\frac{\partial K}{\partial z'}(z_l,r_l;0,r'),$$

$$N1+1\leqslant l\leqslant N1+N2,\ 0\leqslant n\leqslant N1, \tag{3.8}$$

$$\left.\begin{array}{ll} \mathscr{C}(l,n), & 0\leqslant l\leqslant N1,\ N1+1\leqslant n\leqslant N1+N2 \\ \mathscr{G}(l,n), & N1+1\leqslant l,n\leqslant N1+N2 \end{array}\right\}=\int_{C2} r'\,ds'\,\bar{\psi}_n(s')\frac{\partial K}{\partial \eta'}(z_l,r_l;z',r'), \tag{3.9}$$

$$\mathscr{D}(N1+1,N1+1)=\tfrac{1}{2}$$

$$\mathscr{D}(l,l)=1, \qquad N1+2\leqslant l\leqslant N1+N2 \tag{3.10}$$

$$\mathscr{D}(i,j)=0, \qquad N1+1\leqslant i\neq j\leqslant N1+N2.$$

We note that $F(l,n)=0$ for $0\leqslant l\leqslant N1+1$ because $(\partial K/\partial z')\,(0,r;0,r')=0$ for $0\leqslant r\neq r'\leqslant 1$.

If procedure II is used, then row $N1+1$ in CKTOT and CRITE must be changed according to the continuity equation (3.3).

The system (3.4) is solved NCT times with "basis" excitations $\mathbf{A}_0,\ldots,\mathbf{A}_{\mathrm{NCT}-1}$ which satisfy $\mathbf{A}_j(i)=\delta_{ij}$. We call the resulting approximate solutions to (2.5) basis approximate solutions and denote them by $\underline{\phi}^i$ and $\underline{\psi}^i$.

Calculation of the basis far field (or basic first Neumann iterate) is done using the Helmholtz' formula:

$$
\begin{aligned}
F^i(z, r) \cdot 2, \quad & (z, r, \theta) \text{ in } \Omega \\
\cdot 1, \quad & (z, r) \in C1 + C2 - (C1 \cap C2) \\
\cdot \tfrac{1}{2}, \quad & (z, r) = C1 \cap C2 \\
= & -\int_0^1 r'\, dr' \frac{\partial \underline{\phi}^i}{\partial z'}(0, r')\, K(z, r; 0, r') \\
& + \int_0^1 r'\, dr'\, \underline{\phi}^i(0, r') \frac{\partial K}{\partial z'}(z, r; 0, r') \\
& - \int_{C2} r'\, ds'\, \underline{\psi}^i(z', r') \frac{\partial K}{\partial \eta'}(z, r; z', r'). \qquad (3.11)
\end{aligned}
$$

Given the coefficients $A(0),..., A(\mathrm{NCT}-1)$ of the desired excitation, we find the corresponding approximate solution to (2.5) and the far field (or first Neumann iterate) from

$$
\underline{\phi} = \sum_{i=0}^{\mathrm{NCT}-1} A(i)\, \underline{\phi}^i, \qquad \underline{F} = \sum_{i=0}^{\mathrm{NCT}-1} A(i)\, \underline{F}^i. \qquad (3.12)
$$

The initial choice of $N1$ and $N2$ in (3.1) and (3.2) may not always be consistent with the desired accuracy. Also, the equispacing of the knots with respect to the parameter t is usually suboptimal. Section 6 discusses rules for choosing $N1$ and $N2$ initially. We now present a procedure (see [7]) which uses the first approximate solution obtained to estimate the absolute error at the knots, and then recommends new values for $K2$, $K3$, $K4$, and $K5$ and a new distribution of the knots. The goal is to equally distribute the absolute error among the knots and to achieve a desired accuracy.

Let us explain this procedure for BC which is initially divided into $K2$ subintervals. Let t_i denote an interior knot and let h_i and h_{i+1} denote the mesh spacing immediately to the left and right of t_i. Set $h = \max\{h_i, h_{i+1}\}$. At t_i we estimate the second derivative with respect to t of the jth basis approximate solution to (2.5) by interpolation with a parabola at t_{i-1}, t_i, and t_{i+1}. Denote this estimate by d_i^j and set $d_i = \max\{|d_i^j|: 0 \leqslant j \leqslant \mathrm{NCT}-1\}$. We estimate the absolute error at t_i by $d_i h^2/2$. Let AE denote the sum of the errors at the interior knots divided by the number of interior knots, $K2-1$. Let AER denote the desired absolute error, and set

$$
L2 = [K2/\sqrt{\mathrm{AER}/\mathrm{AE}}] + 1,
$$

unless the result is 1, in which case set $L2 = 2$.

Next, we partition BC into $L2$ subintervals so that the error is approximately the same at all interior knots. Set $p = K2$ and $l = L2$ and let $t_1,..., t_{p+1}$ denote the initial knots on BC. Set $u_1 = t_1$, $u_i = (t_i + t_{i+1})/2$, $i = 2,..., p-1$, $u_p = t_{p+1}$. Let G denote

the piecewise constant function defined by $G(t)=\sqrt{d_{i+1}}$ for $u_i<t<u_{i+1}$. For $u_1\leqslant u\leqslant u_p$, define

$$y=\int_{u_1}^{u} G(t)\,dt \qquad \text{and} \qquad y_p=\int_{u_1}^{u_p} G(t)\,dt.$$

Now y is increasing in u so let $u=H(y)$ denote the inverse function. Construct $l+1$ new knots according to $\omega_1=t_1$, $\omega_i=H((i-1)\,y_p/l)$, $i=2,\ldots,l$, $\omega_{l+1}=t_{p+1}$. This procedure is based on our observation that in this problem the redistribution of a fixed number of knots has little effect on the average error AE.

4. Programming Notes

In Fig. 2 curve BC is the arc of an ellipse and curve CD is a line segment. Curve BCD is the exact test inlet contour, while curve DEF is an artificial termination for the inlet. We observed that changing the length of DE did not change the accurate digits in the computed reflection coefficients or in the computed acoustic pressure for $z\geqslant 0$. This was also true if E was replaced by $\tilde{E}$ so that $D\tilde{E}$ is a horizontal line segment and $\tilde{E}F$ is a quarter arc of a circle; i.e., the introduction of a corner at point D had an insignificant effect on the numerical results. The results reported below are for the computational exterior inlet contour $BCD\tilde{E}F$ which is an approximation to the smooth contour $BCDEF$ shown in Fig. 2.

Almost all the execution time of our code is devoted to the subroutine which assembles the complex matrices CKTOT and CRITE in (3.4). The difficulty is that the oscillatory and singular double integrals in (3.7)–(3.9) must be computed. We use adaptive integration which is ideal for this type of behaviour, but expensive. Alternatively, we could have developed a suitable product formula and then used the Nystrom method instead of collocation.

We have separated the integrands in (3.7)–(3.9) into a bounded part and a singular part corresponding to the axisymmetric potential equation.

Let $\rho=((r'-r_l)^2+(z'-z_l)^2)^{1/2}$ and $\bar{\rho}=((r'+r_l)^2+(z'-z_l)^2)^{1/2}$, let $\zeta=kR/2$, $\eta'=(N_{z'}, N_{r'})$, and let $\mathscr{K}$ and $\mathscr{E}$ denote the complete elliptic integrals of the first and second kinds as functions of the complementary parameter $m_1=\rho^2/\bar{\rho}^2$ (see [8, 9]).

Then in (3.7) we have

$$\mathscr{B}(l,n)=-\frac{iL(n)}{\pi}\int_0^1 r'\,dr'\,J_m(\lambda(n)\,r')$$

$$\times\int_0^{\pi} dY(\cos(mY)(e^{ikR}-1)+\cos(mY)-1)/R$$

$$-\frac{iL(n)}{\pi}\int_0^1 r'\,dr'\,J_m(\lambda(n)\,r')\int_0^{\pi}\frac{dY}{R}$$

$$= -\frac{iL(n)\,k}{\pi}\int_0^1 r'\,dr'\,J_m(\lambda(n)\,r')$$

$$\times\int_0^\pi dY(i\cos(mY)\sin(\zeta)\,e^{i\zeta}-\sin^2(mY/2))/\zeta$$

$$-\frac{2iL(n)}{\pi}\int_0^1 r'\,dr'\,J_m(\lambda(n)\,r')\,\mathscr{K}(m_1)/\bar{\rho},$$

while in (3.9) we have

$$\mathscr{C}(l,n)=\pi^{-1}\int_{C2} r'\,ds'\,\bar{\psi}_n(s')$$

$$\cdot\int_0^\pi dY\left(\cos(mY)\frac{\partial}{\partial\eta'}\left(\frac{e^{ikR}-1}{R}\right)+(\cos(mY)-1)\frac{\partial}{\partial\eta'}\frac{1}{R}\right)$$

$$+\pi^{-1}\int_{C2} r'\,ds'\,\bar{\psi}_n(s')\int_0^\pi dY\frac{\partial}{\partial\eta'}\frac{1}{R}$$

$$=\frac{k^2}{2\pi}\int_{C2} r'\,ds'\,\bar{\psi}_n(s')$$

$$\cdot\int_0^\pi dY(N_{z'}(z'-z_l)+N_{r'}(r'-r_l+2r_l\sin^2(Y/2)))$$

$$\cdot\left\{i\cos(mY)\,e^{i\zeta}\left(\frac{\zeta\cos\zeta-\sin\zeta}{\zeta^2}+i\frac{\sin\zeta}{\zeta}\right)+\left(\frac{\sin(mY/2)}{\zeta}\right)^2\right\}$$

$$+\pi^{-1}\int_{C2} ds'\,\frac{\bar{\psi}_n(s')}{\bar{\rho}}$$

$$\cdot\{2r'\mathscr{E}(m_1)(N_{r'}(r_l-r')+N_{z'}(z_l-z'))/\rho^2+N_{r'}(\mathscr{E}(m_1)-\mathscr{K}(m_1))\}.$$

For the evaluation of J_1, J_m, $m\geq 2$, $\mathscr{K}(m_1)$, and $\mathscr{E}(m_1)$ we use the LRC library routines BJ1R, BKIR, ELIPKC, and ELIPEC. For the evaluation of the one-dimensional integrals we use the LRC library routine CADRE which is a modification of an algorithm due to de Boor [10]. For the double integrals we use the LRC library routine CAREDB which computes the integral as iterated single integrals with the single integrals computed as in CADRE.

CADRE is an adaptive cautious Romberg extrapolation routine which is designed to identify certain tyes of integrand behaviour by examining a ratio based on the previous three trapezoidal sums. We split the integrals so that the singularities are endpoint singularities. If such a singularity is detected, CADRE switches to a process similar to Aitken's δ^2 process to estimate the integral and evaluate the error. As a result of this switching, we have observed that execution times decrease with the error tolerances. We use EPS(1) = EPS(2) = $E-5$, where

EPS(1) is the maximum allowable relative error and EPS(2) the maximum allowable error. These remarks also hold for CAREDB. Adaptive integration is particularly suited to oscillatory and (or) singular integrals. It offers the possibility of constructing a test code for an integral equation method in a relatively short time.

Once the linear system (3.4) is assembled, it is solved using the LRC library routine CXGCOIT. This subroutine performs an LU decomposition, solves by forward and backward substitution, and estimates the condition number (CONDNUM) of CKTOT in the 1-norm. Optionally, iterative refinement can be performed (see [11]). For more details see [12].

5. Numerical Results

All computations were performed on a CDC Cyber 175 at NASA Langley Research Center. We give results for the programs which collocate at $C1 \cap C2$ instead of demanding the continuity equation (3.3) hold. We have found little difference in the outputs of these two sets of programs.

For a given azimuthal mode index m, it is best to start with a value of $k = \bar{k}a$ so that one mode is cuton (NCT = 1) and then increase k to the desired level. Good starting values then are $N1 = \text{NCT} + 5$ and $K2 = 20$, $K3 = 10$, $K4 = 10$, $K5 = 7$. Our code recommends new values for $K2,\ldots, K5$ with respect to a user-supplied tolerance. The user has the option of running the code again with these new values. We have provided a continuity check which outputs the modulus of the difference in the two sides of (3.3) for an approximate solution. If this continuity check is greater than the error tolerance, then $N1$ can be increased. The error estimates on $C2$ and the continuity check are a reasonable indication of the accuracy attained. Of course, the condition number and the accuracy with which CKTOT and CRITE are computed must also be considered.

Tables I and II present some of our numerical results. Table I shows results for $m = 1$ and $k = \bar{k}a = 2.66$ and an increasing sequence of values for $N1 + N2$. CONT is the value of the continuity check. The error in $|R(0)|$ and the error at $C1 \cap C2$ are estimated by comparison with the case $N1 + N2 = 78$.

TABLE I

$N1$	$N2$	CONDUM	CONT	$\lvert R(0)\rvert$	Angle $R(0)$	Error $\lvert R(0)\rvert$	Error $C1 \cap C2$	Maximum Error est. $C2$
6	18	29	0.0016	0.3555	−20.76	0.011	0.0077	0.0080
2	34	26.8	0.006	0.3479	−20.13	0.0029	0.0012	0.0021
6	34	34.1	0.00076	0.3476	−20.17	0.0027	0.0015	0.0019
10	34	41.2	0.00044	0.3475	−20.17	0.0026	0.0019	0.0019
6	68	47.9	0.0011	0.3451	−20.00	0.000043	0.00037	0.00051
10	68	54.2	0.00038	0.3451	−20.00			

TABLE II

Max Far Field SPL = 0 dB

$k = \bar{k}a$	Coefficient	Numerical dB	Angle (°)	Experimental dB
2.66	$A(0)$	36.0	0	36.1
	$R(0)$	26.8	−20.2	27.0
3.20	$A(0)$	33.8	0	32.6
	$R(0)$	18.1 ± 0.2	25.2	18.5
5.54	$A(0)$	24.4	−8.4	25.8
	$R(0)$	2.2 ± 1.64	29.8	18.3
	$A(1)$	37.8	−139.1	39.2
	$R(1)$	28.5	141.3	29.6
6.50	$A(0)$	23.9	70.4	22.9
	$R(0)$	-9.2 ± 4.3	19.9	9.9
	$A(1)$	34.5	−64	33.5
	$R(1)$	-1.3 ± 1.7	−54	9.9
7.68	$A(0)$	23.4	−159.6	23.5
	$R(0)$	-5.4 ± 2.2	−168.2	3.4
	$A(1)$	33.0	56.6	33.1
	$R(1)$	-4 ± 1.2	−5.7	9.5

Table II gives for $m = 1$ a comparison of experimental and numerical results for $k = 2.66$, 3.20, 5.54, 6.50, and 7.68. Some of these results are in close agreement; for example, for $k = 2.66$, we have $|R(0)|/|A(0)| = 0.348$ (numerical) and 0.35 (experimental). However, for $k = 3.20$, we have $|R(0)|/|A(0)| = 0.164$, while the experimental value is 0.196. Our error tolerance here is 0.002. The continuity check and error estimates on $C2$ are consistent with this tolerance. Generally, when $R(i)$ is small compared to $\max\{|A(0)|,..., |A(\mathrm{NCT}-1)|\}$, we have the greatest relative error. We have indicated the error bracket on some of these entries in Table II. But

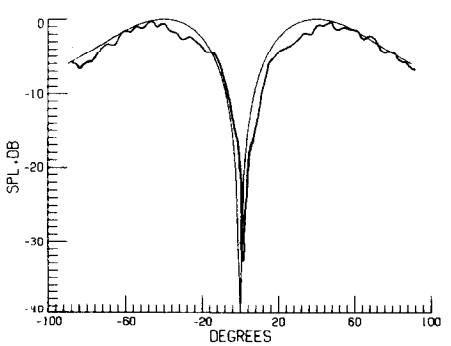

FIG. 3. $m = 1$, $k = 2.66$, NCT = 1.

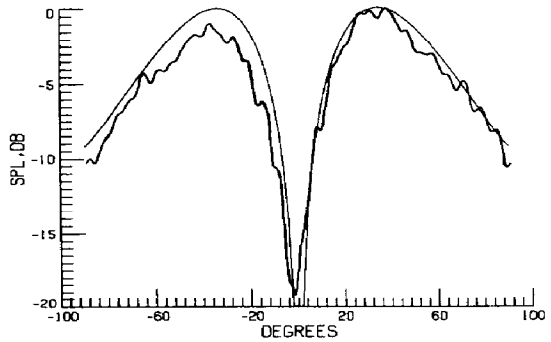

FIG. 4. $m = 1,\ k = 3.20,\ \mathrm{NCT} = 1.$

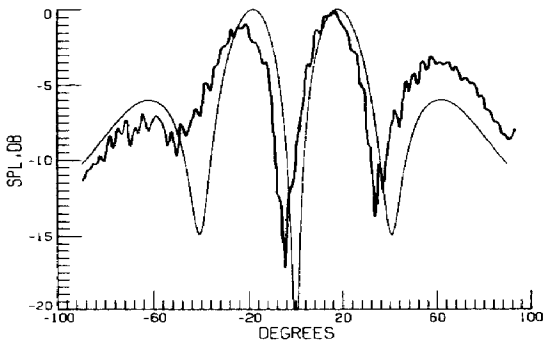

FIG. 5. $m = 1,\ k = 5.54,\ \mathrm{NCT} = 2.$

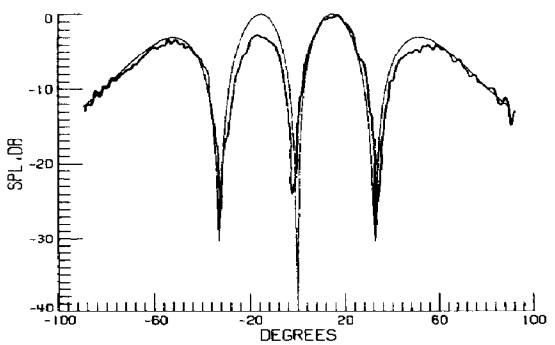

FIG. 6. $m = 1,\ k = 6.50,\ \mathrm{NCT} = 2.$

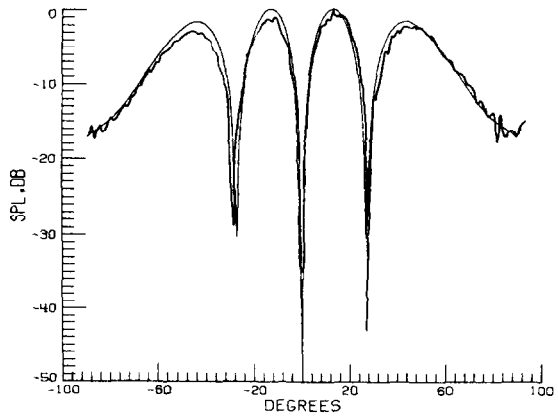

FIG. 7. $m = 1$, $k = 7.68$, NCT = 2.

these brackets do not account for some of the discrepancies. We note that the dB levels in Table II are referenced so that the peak sound pressure level in the far field is 0 dB (for both experimental and numerical results).

Figures 3, 4, 5, 6, and 7 give far field patterns computed on a semicircle of radius 20 in front of the duct (see Fig. 1). We note the good agreement between the numerical and experimental curves. The small oscillations in the experimental curve may be due to reflections, while the lack of symmetry indicates less than complete isolation of the desired arimuthal mode. We compute and store a basis approximate solution and far field. Then we can interactively produce approximate solutions and far field patterns for any given excitation strengths $A(0),..., A(\text{NCT}-1)$. Thus we have an NCT parameter family of possible far fields that can be generated quickly. It is possible, for example, to make the -30 dB downward spikes in the $k = 6.50$ case almost completely disappear by choice of excitation strengths. But roughly speaking, these different patterns have the same "envelope."

We have experimented with the best location for the interface surface $S1$. This is a trade-off between the two types of approximation—Bessel series and piecewise linear spline. The best efficiency is obtained by using the modal expansion over as large a region as possible.

6. UNIQUENESS

We conclude by showing that a slight modification of the standard proof shows that uniqueness holds for the boundary value problem of Section 2. In this section we will use subscript notation for partial derivatives. Let w denote the difference of two solutions to this boundary value problem. Then w is in class $C^2(\Omega) \cap C^1(\bar{\Omega})$,

$\Delta w + k^2 w = 0$, in Ω, with k real, the normal derivative of w vanishes on $S2$, w satisfies the radiation condition at infinity, and

$$w = \sum_{n=0}^{\infty} R(n)\, J_m(\lambda(n)\, r)\, e^{im\theta}, \qquad z = 0,\ 0 \leqslant r \leqslant 1,$$

and

$$w_z = \sum_{n=0}^{\infty} (-iL(n))\, R(n)\, J_m(\lambda(n)\, r)\, e^{im\theta}, \qquad z = 0,\ 0 \leqslant r \leqslant 1.$$

Let S_ρ denote the sphere of radius ρ centered at the origin. Then there is a $\rho_0 > 0$ so that $S1 + S2$ is in the interior of S_ρ for all $\rho \geqslant \rho_0$. For $\rho \geqslant \rho_0$ let Ω_ρ denote the domain interior to S_ρ and exterior to $S1 + S2$. The Green's second identity applied to w and $\bar{w}$, the conjugate of w, yields

$$0 = \int_{\Omega_\rho} (w\, \Delta\bar{w} - \bar{w}\, \Delta w)\, dx = \int_{S1 + S2 + S_\rho} (w\bar{w}_\eta - \bar{w}w_\eta)\, dS,$$

where η denotes the normal pointing out of Ω_ρ. It follows that

$$\begin{aligned}\int_{S_\rho} (\bar{w}w_\rho - w\bar{w}_\rho)\, dS &= \int_{S1} (\bar{w}w_z - w\bar{w}_z)\, dS \\ &= -4\pi i \sum_{n=0}^{\mathrm{NCT}-1} (k^2 - \lambda(n))^{1/2}\, |R(n)|^2 \int_0^1 r\, dr (J_m(\lambda(n)\, r))^2.\end{aligned}$$

Now w satisfies the radiation condition at infinity hence $\lim_{\rho \to \infty} R(\rho) = 0$ where

$$\begin{aligned}R(\rho) &= \int_{S_\rho} |w_\rho - ikw|^2\, dS \\ &= \int_{S_\rho} |w_\rho|^2\, dS + k^2 \int_{S_\rho} |w|^2\, dS + ik \int_{S_\rho} (\bar{w}w_\rho - w\bar{w}_\rho)\, dS.\end{aligned}$$

These last two equations yield

$$R(\rho) = \int_{S_\rho} |w_\rho|^2\, dS + k^2 \int_{S_\rho} |w|^2\, dS + kC$$

where $C \geqslant 0$ is a constant independent of ρ. It follows that

$$\lim_{\rho \to \infty} \int_{S_\rho} |w|^2\, dS = 0.$$

But then the first lemma of F. Rellich [13] implies that w vanishes for $\rho > \rho_0$. Since Ω is connected and w is analytic, it follows that w vanishes in Ω. This completes the uniqueness proof.

REFERENCES

1. J. M. VILLE AND R. J. SILCOX, NASA TP-1697, 1980.
2. R. J. SILCOX, *AIAA-83-0713*, (1983).
3. K. J. BAUMEISTER, NASA Technical Memorandum 82730, 1981.
4. D. L. PALUMBO, NASA Contractor Report 165698, 1981.
5. Y. KAGAWA, T. YAMABUCHI, T. YOSHIKAWA, S. OOIE, N. KYOUNO, AND T. SHINDOU, *J. Sound Vibration* **69** (2), 207–228 (1980).
6. W. L. MEYER, W. A. BELL, B. T. ZINN, AND M. P. STALLYBRASS, *J. Sound Vibration* **59** (2), 245–262 (1978).
7. C. DE BOOR, *A Practical Guide to Splines* (Springer-Verlag, New York/Berlin, 1978).
8. M. ABRAMOWITZ AND I. A. STEGUN, *Handbook of Mathematical Functions*, NBS Applied Mathematics Series 55 (U.S. Gov. Printing Office, Washington, D.C., 1981).
9. D. J. SHIPPY, F. J. RIZZO, AND A. K. GUPTA, *Dev. Theor. Appl. Mech.* **10**, 189–206 (1980).
10. C. DE BOOR, "CADRE: Algorithm for Numerical Quadrature," *Mathematical Software*, edited by J. R. Rice (Academic Press, New York/London, 1971).
11. J. J. DONGARRA, J. R. BUNCH, C. B. MOLER, AND G. W. STEWART, *LINPACK User's Guide* (SIAM, Philadelphia, 1979).
12. W. F. MOSS, NASA Contractor Report 172273, 1983.
13. G. HELLWIG, *Partial Differential Equations* (Ginn (Blaisdell), New York, 1964).
14. A. J. BURTON, "Numerical Solution of Scalar Diffraction Problems," *Numerical Solution of Integral Equations*, edited by L. M. Delves and J. Walsh (Oxford Univ. Press (Clarendon), Oxford, 1974).
15. M. A. HAMDI, *C. R. Acad. Sci. Ser. B* **292**, 17–20 (1981).
16. R. E. KLEINMAN AND R. KRESS, *IMA J. Appl. Math.* **31**, 79–90 (1983).
17. R. E. KLEINMAN AND G. F. ROACH, *Proc. R. Soc. London Ser. A* **383**, 313–332 (1982).
18. D. S. JONES, *Quart. J. Mech. Appl. Math.* **27**, 129–142 (1974).
19. F. URSELL, *Proc. Cambridge Philos. Soc.* **84**, 545–548 (1978).